PNAS RESEARCH ARTICLE | CELL BIOLOGY

OPA1 disease-causing mutants have domain-specific effects on mitochondrial ultrastructure and fusion

Benjamín Cartes-Saavedra[a,b,1], Daniel Lagos[a,1], Josefa Macuada[a], Duxan Arancibia[a,c], Florence Burté[d], Marcela K. Sjöberg-Herrera[a], María Estela Andrés[a], Rita Horvath[e], Patrick Yu-Wai-Man[e,f,g,h,i], György Hajnóczky[b], and Verónica Eisner[a,2]

Edited by Antonio Zorzano, Institut de Recerca Biomedica, Barcelona, Spain; received May 12, 2022; accepted January 23, 2023 by Editorial Board Member Francisco Bezanilla

Inner mitochondrial membrane fusion and cristae shape depend on optic atrophy protein 1, OPA1. Mutations in *OPA1* lead to autosomal dominant optic atrophy (ADOA), an important cause of inherited blindness. The Guanosin Triphosphatase (GTPase) and GTPase effector domains (GEDs) of OPA1 are essential for mitochondrial fusion; yet, their specific roles remain elusive. Intriguingly, patients carrying *OPA1* GTPase mutations have a higher risk of developing more severe multisystemic symptoms in addition to optic atrophy, suggesting pathogenic contributions for the GTPase and GED domains, respectively. We studied *OPA1* GTPase and GED mutations to understand their domain-specific contribution to protein function by analyzing patient-derived cells and gain-of-function paradigms. Mitochondria from *OPA1* GTPase (c.870+5G>A and c.889C>T) and GED (c.2713C>T and c.2818+5G>A) mutants display distinct aberrant cristae ultrastructure. While all OPA1 mutants inhibited mitochondrial fusion, some GTPase mutants resulted in elongated mitochondria, suggesting fission inhibition. We show that the GED is dispensable for fusion and OPA1 oligomer formation but necessary for GTPase activity. Finally, splicing defect mutants displayed a posttranslational haploinsufficiency-like phenotype but retained domain-specific dysfunctions. Thus, OPA1 domain-specific mutants result in distinct impairments in mitochondrial dynamics, providing insight into OPA1 function and its contribution to ADOA pathogenesis and severity.

mitochondria | OPA1 | ADOA | dynamics | cristae

Mitochondria undergo constant restructuring by fusion, fission, and cristae reshaping. These support bioenergetic function and cellular fate decisions (1–3), helping the cell to adapt to various genetic and environmental conditions (4, 5). The fusion of two contiguous mitochondria involves sequential mixing of the outer membrane (OMM), intermembrane space, inner membrane (IMM), and the matrix components (6, 7). Fusion is required to rescue damaged mitochondria by supporting mitochondria DNA (mtDNA) stability and replication (3, 8), complementation of OMM components (9), and cristae biogenesis (10). Fusion is orchestrated by MFN1/MFN2 (6) and OPA1 proteins (11), assisting OMM and IMM fusion, respectively (6). These proteins are members of the dynamin-related protein family, which displays conserved GTPase and GTPase effector domains (GED) (12).

OPA1 is a nuclear gene that encodes eight different isoforms (gene ID: 4876). Splice sites 1 and 2 are relevant for protein processing and lead to long and short forms of OPA1 (13, 14). Originally linked to IMM fusion (15), OPA1 plays additional roles in cristae maintenance (16) and mitochondrial fission (17). OPA1 facilitates IMM fusion by means of a GTP-coupled reaction and interaction with cardiolipin (18, 19). To support cristae biogenesis and cristae junction maintenance, OPA1 interacts with the mitochondrial contact site and cristae organizing system (MICOS) complex (20, 21). The different domains of the OPA1 protein are involved in distinct functions. For example, the coiled-coil domain 1 is important for protein–protein interaction, and the GTPase domain is relevant for fusion activity (22); while the GED region, predicted as coiled-coil domain 2, is required to assist the GTPase activity (23). Although all 8 OPA1 isoforms carry both GTPase and GED domains (24) and have redundant roles on mitochondrial ultrastructure, only the long forms of OPA1 rescue mitochondrial fusion in *Opa1* null cells (25). We recently showed that the OPA1 GED region determines endoplasmic reticulum-to-mitochondria Ca^{2+} transference (26). An open question remaining in the field is whether the GTPase and GED regions have specific contributions to the roles of OPA1 in IMM fusion, cristae maintenance, or fission.

The complete absence of OPA1 is incompatible with life, as demonstrated by the embryonic lethality of *Opa1* knock-out mice (27). Heterozygous *OPA1* mutations lead to autosomal dominant optic atrophy (ADOA, Mendelian Inheritance in Man (MIM)

Significance

OPA1 mediates inner mitochondrial membrane dynamic reshaping, and mutations affecting this protein cause autosomal dominant optic atrophy (ADOA), a leading cause of inherited blindness. This study explored *OPA1* GTPase and GTPase effector domain (GED) mutants. The domain-specific *OPA1* mutants exhibited distinctive ultrastructural cristae defects. *OPA1* mutants carrying GED defects retained partial fusion activity and partial GTPase function. In comparison, defects in mitochondrial fusion and fission were observed in GTPase mutants, which are linked to more severe multisystemic forms of ADOA. These contrasting effects on mitochondrial dynamics could account for the diverse mitochondrial morphology phenotypes observed. Thus, our data highlight each domain's contribution to OPA1 dysfunction and might provide clues to the factors driving ADOA pathogenesis and severity.

The authors declare no competing interest.

This article is a PNAS Direct Submission. A.Z. is a guest editor invited by the Editorial Board.

[1]B.C.-S. and D.L. contributed equally to this work.

[2]To whom correspondence may be addressed. Email: veisner@bio.puc.cl.

This article contains supporting information online at https://www.pnas.org/lookup/suppl/doi:10.1073/pnas.2207471120/-/DCSupplemental.

Published March 16, 2023.

165500). This disease is characterized by progressive retinal ganglion cell loss, resulting in optic nerve degeneration and visual failure (28). ADOA is the most common form of inherited optic neuropathy, with an estimated prevalence of one in 25,000 births (29). ADOA is subclassified as ADOA plus (ADOA+, MIM: 125250) when other neurological symptoms are present, such as sensorineural hearing loss, muscle weakness, and ataxia (30, 31). Over 400 different pathogenic *OPA1* variants with a wide range of clinical features have been described in the Leiden Open Variation Database (LOVD) (32), or the ClinVar Database (33). Interestingly, missense mutations involving the GTPase domain are associated with a higher risk of developing ADOA+ compared with other regions (29, 30), but the mechanisms driving this increased susceptibility remain unknown.

To gain insights into the differential contributions of the GTPase and the GED domains to the different functions of OPA1 and their contribution to the development of ADOA and ADOA+ phenotypes, we set out to study a panel of GTPase and GED mutant-bearing cells from patients. To substantiate our findings, we also tested each mutant in *Opa1* null or wild-type (WT) mouse embryonic fibroblasts (MEFs). We comprehensively tested mitochondrial reshaping proteins, ultrastructure, and mitochondrial fusion dynamics, which allowed us to establish the domain-specific effects of *OPA1* mutations and their phenotypic consequences.

Results

Studies on ADOA Patient-Derived Cells.

OPA1 GTPase and GED mutations show different profiles for mitochondrial dynamics proteins. We analyzed fibroblast or myoblasts established from patients carrying heterozygous mutations in *OPA1*, particularly in the GTPase and GED domains, and displayed different severities of ADOA (*SI Appendix*, Fig. S1*A*). We analyzed two GTPase mutants from patients manifesting an ADOA+ phenotype, an *OPA1* splicing defect c.870+5G>A/p.Lys262_Arg290Del that causes the loss of exon 8, and an *OPA1* nonsense mutation c.889C>T/p.Gln297X. We also studied two GED mutants from patients exhibiting a pure ADOA phenotype, an *OPA1* nonsense mutation c.2713C>T/p.Arg905X, and an *OPA1* splicing defect c.2818+5g>a/p.Val903_Lys940Del_InsGlu that causes the loss of the exon 27 (*SI Appendix*, Fig. S1*A*). Skeletal muscle-derived fibroblasts were used for most experiments. As those carrying the *OPA1*c.889C>T mutation did not grow in normal conditions, we thus used skin-derived fibroblasts from the same patient.

Western blot analysis of whole-cell protein extracts from patient cells carrying GTPase domain mutants *OPA1*c.870+5G>A and c.889C>T showed lower OPA1 levels compared to control cells (Fig. 1 *A* and *B* and *SI Appendix*, Fig. S1*B*). The *OPA1*c.889C>T mutation leads to a truncated form of OPA1 (Fig. 1*C*), which was undetectable by commercial antibodies (details in *Materials and Methods*). However, we cannot discard the complete absence of the mutated allele, as the escape from the nonsense-mediated messenger RNA (mRNA) decay system has been described for the N-terminal stop codon mutant for OPA1 (34, 35). Cells carrying the *OPA1*c.2818+5G>A mutation in the GED domain also display lower OPA1 levels, while no change was found for the *OPA1*c.2713C>T mutation (Fig. 1 *A* and *B* and *SI Appendix*, Fig. S1*B*).

We next surveyed MFN1 and MFN2 because they act together with OPA1 in mitochondrial fusion (4), and MFN2 has its own disease relevance (36). Both GED mutants showed significantly increased MFN2 protein levels (Fig. 1*A* and *SI Appendix*, Fig. S1*B*). MFN1 levels were significantly increased only in cells

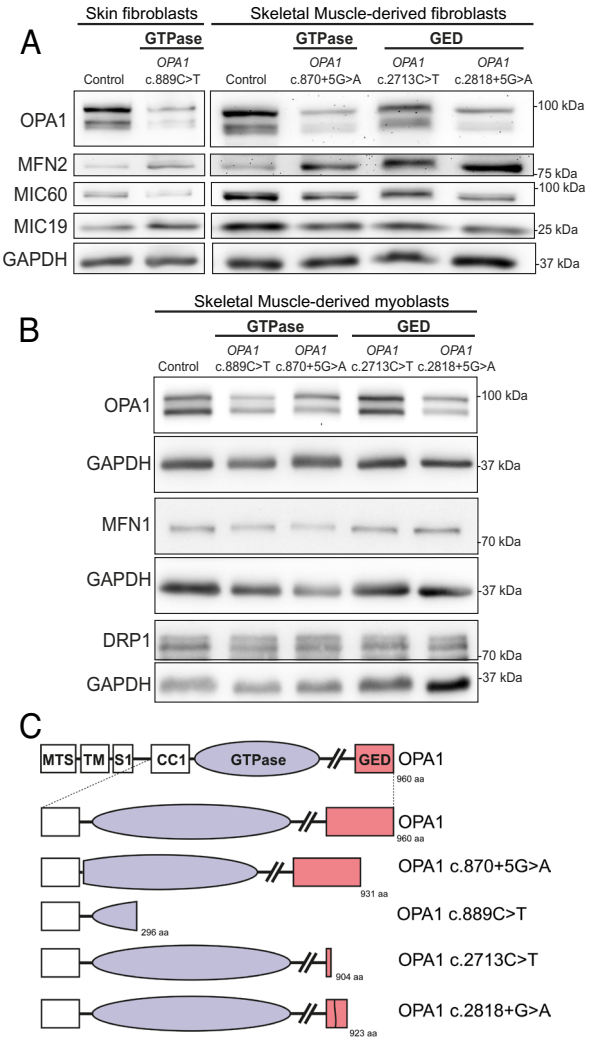

Fig. 1. ADOA-causing mutants located at GTPase and GED domain differentially alter mitochondrial reshaping proteins in patient-derived fibroblasts. (*A* and *B*) Western blot analysis of whole-cell extracts from ADOA-derived fibroblast or myoblasts, representative images. (*C*) Representation of OPA1, primary structure indicating specific domains, based on the result of polypeptide sequence (isoform 1), showing the location of ADOA-causing mutations described in *A*. MTS, mitochondrial targeting sequence; TM, transmembrane domain; S1, processing site 1; GTPase, GTPase domain; GED, GTPase effector domain.

carrying the mutation *OPA1*c.2818+5G>A (Fig. 1*B* and *SI Appendix*, Fig. S1*B*). We also tested DRP1 levels, the main effector on mitochondrial fission, with no statistical difference between the patients and control cells (Fig. 1*B* and *SI Appendix*, Fig. S1*B*). MIC60 and MIC19 are components of the MICOS complex that is essential for IMM and cristae organization and are known to interact with OPA1 (37). MIC60 levels were decreased in most OPA1 mutants, while levels of MIC19 changed only in the c.870+5G> *OPA1* mutant (Fig. 1*A* and *SI Appendix*, Fig. S1*B*).

Given that the splicing defects caused by *OPA1*c.870+5G>A and *OPA1*c.2818+5G>A display decreased OPA1's protein levels, we next checked the transcriptional levels of the mutants. mRNA was isolated and analyzed by semi-quantitative RT-PCR with primers flanking exons 8 and 27, covering both WT and the splicing variants. We detected a single band of mRNA for WT OPA1 and two bands in the spliced variants with the deletions of the exon 8 (*OPA1*c.870+5G>A) and exon 27 (*OPA1*c.2818+5G>A), respectively (*SI Appendix*, Fig. S1*C*), consistent with the patient's

heterozygosity. These data show that mRNA of the different mutants is not degraded, suggesting that the decrease in OPA1 protein levels is posttranslational.

In silico splicing analysis of OPA1 mutants c.870+5G>A and c.2818+5G>A confirmed that the intronic mutations alter the donor splice site of the exons 8 and 27, respectively, explaining the loss of these exons, which lead to shorter transcripts (*SI Appendix*, Fig. S1 *C–F*). Also, in *OPA1*c.870+5G>A, no GTPase motifs (G1-5) were mutated.

These results suggest that the mutations present in the different ADOA-derived cells display dissimilar profiles for the actors of mitochondrial fusion-fission. OPA1 and MIC60 proteins were down-regulated in the GTPase mutants and *OPA1*c.2818+5G>A. Conversely, MFN1 and MFN2 were increased in GED mutants, raising the possibility that exclusive optic nerve–degenerating mutants may try to cope with mitochondrial dysfunction by a compensatory increase of the mitofusins.

Cells carrying GTPase and GED mutations display different mitochondrial morphology and cristae shape alterations. In transmission electron microscopy (TEM) analysis, the total mitochondrial area and the frequency of larger mitochondria were increased in cells from patients carrying either *OPA1* GTPase or GED mutations (Fig. 2 *A* and *B*). In addition, all patient cells showed a significant increase in aberrant mitochondrial shape (*SI Appendix*, Fig. S2 *A* and *B*). Cells carrying GTPase mutations exhibited partial matrix swelling and cristae interruptions, whereas mitochondria from patients carrying GED mutations showed swollen mitochondria (Fig. 2*A*) Both GTPase and GED mutants displayed cristae aberrations such as vesicular-, arc-, and onion-shaped cristae and an increase in the abundance of mitochondria with short cristae (*SI Appendix*, Fig. S2 *C* and *D*). This might be a consequence of the decline in MIC60 or OPA1 levels in most mutants, except cells carrying c.2713C>T (Fig. 1*A*).

Given the differential expression of OPA1 and MIC60, cristae junction width and cristae lumen width were analyzed (Fig. 2*C*). All mitochondria from ADOA-derived fibroblasts showed a significant increase in cristae junction width (Fig. 2*D*). However, cristae lumen width increased only in patients carrying a mutation in the GED domain (Fig. 2*E*). Unexpectedly, cells carrying GTPase mutations showed a decrease or no change in the cristae lumen width (Fig. 2*E*).

Thus, TEM analysis of ADOA-derived fibroblasts revealed enlarged mitochondria with distinct cristae perturbations for GTPase and GED-carrying mutants. Semiquantitative analysis of cristae structure demonstrated defects in the closure of cristae

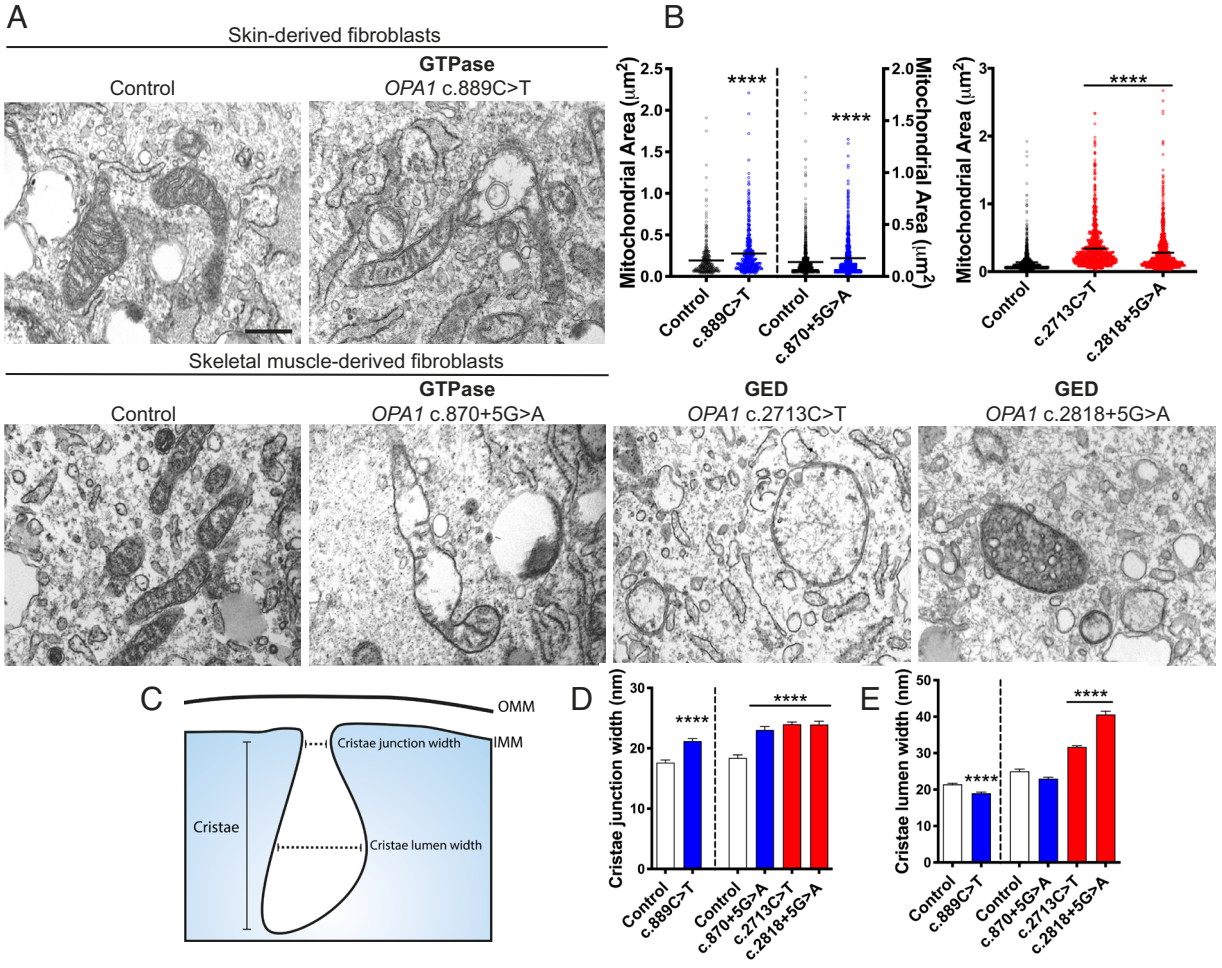

Fig. 2. Mitochondrial ultrastructure of ADOA patient-derived cells carrying GTPase and GED mutations displays dissimilar aberrations in organelle morphology, and cristae shape. (*A*) Representative TEM images of mitochondria from ADOA-derived fibroblast. (Scale bar, 500 nm.) (*B*) Total mitochondrial area quantification. (Control skin, n = 2/19/345; preparations/cells/mitochondria), (*OPA1*c.889C>T, n = 2/30/411), (control SkM, n = 3/17/1,973), (*OPA1*c.870+5G>A, n = 3/25/982), (*OPA1*c.2713C>T, n = 3/28/1,223), (*OPA1*c.2818+5G>A. n = 2/18/1,128). (*C*) Schematic representation of an individual crista. The short dash line indicates how cristae junction width was measured. The large dash line indicates how cristae lumen width was calculated. (*D*) Cristae junction width analysis. (Control skin, n = 2/69/222; preparations/mitochondria/ CJ), (*OPA1*c.889C>T, n = 2/60/230), (control SkM, n = 3/74/192), (*OPA1*c.870+5G>A, n = 3/65/190), (*OPA1*c.2713C>T, n = 3/112/474), (*OPA1*c.2818+5G>A, n = 2/71/311). (*E*) Cristae lumen width analysis, (control skin, n = 2/113/697; preparations/mitochondria/CL), (*OPA1*c.889C>T, n = 2/102/484), (control SkM, n = 3/83/376), (*OPA1*c.870+5G>A, n = 3/60/335), (*OPA1*c.2713C>T, n = 3/184/1,320), (*OPA1*c.2818+5G>A, n = 2/89/766), Data are mean ± SEM. ****$P < 0.0001$ vs. respective control condition. Blue and red bars represent GTPase and GED mutants, respectively.

junction aperture width in all the ADOA-derived mutants, with a broader lumen present in GED mutants. Cristae perturbations and OPA1 and MIC60 downregulation could partly explain the bioenergetics imbalances and increased susceptibility to apoptosis contributing to this disease (31, 38).

GTPase and GED domain-specific mutants display divergent mitochondrial fusion dynamics. To test mitochondrial morphology and fusion dynamics in live cells, patient-derived fibroblasts were cotransfected with mitochondrial matrix-targeted proteins mt-DsRed and photoactivatable Green fluorescent protein (GFP), Mitochondrial photoactivable green fluorescent protein (mt-PAGFP). Mitochondrial morphology was assessed based on the mt-DsRed distribution. Unexpectedly, the GTPase mutant (*OPA1*c.870+5G>A) exhibited more cells with an elongated mitochondrial network. In contrast, the GED mutant (*OPA1*c.2713C>T) presented a fragmented pattern (Fig. 3 *A* and *B*).

Mitochondrial continuity and fusion frequency analysis involved mt-PAGFP photoconversion as described in *SI Appendix*, *Materials and Methods* (Fig. 3*C*). Mean traces of mt-PAGFP decay analysis showed that GTPase mutant *OPA1*c.870+5G>A displayed a significantly faster decay compared with the control cells (Fig. 3*D*), confirming the presence of an interconnected mitochondrial network suggested by the morphological analysis. GED mutant *OPA1*c.2713C>T showed a significantly slower mt-PAGFP fluorescence decay inside the ROI, compared with the control cells, consistent with fragmented mitochondria (Fig. 3*D*).

Cells from control individuals had 0.79 ± 0.07 fusion events/min (Fig. 3*E*). Cells from ADOA patients with both GTPase and GED mutants displayed a major decrease in fusion activity compared with individual control cells. In *OPA1*c.870+5G>A-carrying cells, this was unexpected considering their elongated mitochondria (Fig. 3*E*). Yet, in these cells, the mitochondria displayed a beads-on-string phenotype (*SI Appendix*, Fig. S3 *A* and *B* and Movie S1), suggesting incomplete fission execution. Our results confirmed that *OPA1*c.870+5G>A displays lower fission activity with no changes in the organelle constriction or organelle fission lag time, implying inefficient fission execution (Fig. 3*F* and *SI Appendix*, Fig. S3 *C–E*). Also, the *OPA1*c.2713C>T-bearing patient cells showed increased fission activity with a lower frequency of organelle constriction, suggesting that the fragmented morphology of this mutant may be a result of decreased fusion and increased fission (Fig. 3*F* and *SI Appendix*, Fig. S3 *C–E*).

The unexpected fact that cells carrying the GTPase mutation c.870+5G>A have lower levels of OPA1 and elongated mitochondria, associated with a lower mitochondrial fusion rate, indicates that the decrease in fission might be larger than the decrease in fusion, determining the elongated mitochondrial shape. Differently, the GED mutant c.2713C>T with unaltered OPA1 protein levels displayed fragmented mitochondria, indicating a dominant negative effect of this mutant on mitochondrial fusion and increased mitochondrial fission activity. Thus, both mutants showed inhibited mitochondrial fusion activity; however, their morphology diverted, suggesting distinct underlying mechanisms.

Acute Rescue Studies with OPA1 Domain-Specific Mutants in *Opa1*$^{-/-}$ and WT MEFs. The patient-derived cells carry different genetic backgrounds and environmental conditioning. To study the specific effects of the mutants present in the patients, we used a plasmid that encodes for human protein OPA1 isoform 1 (*OPA1*), considering that this is the most abundant isoform in HeLa cells, human, and mouse tissues (14, 39). As we previously reported (26), we edited the OPA1-encoding complementary DNA

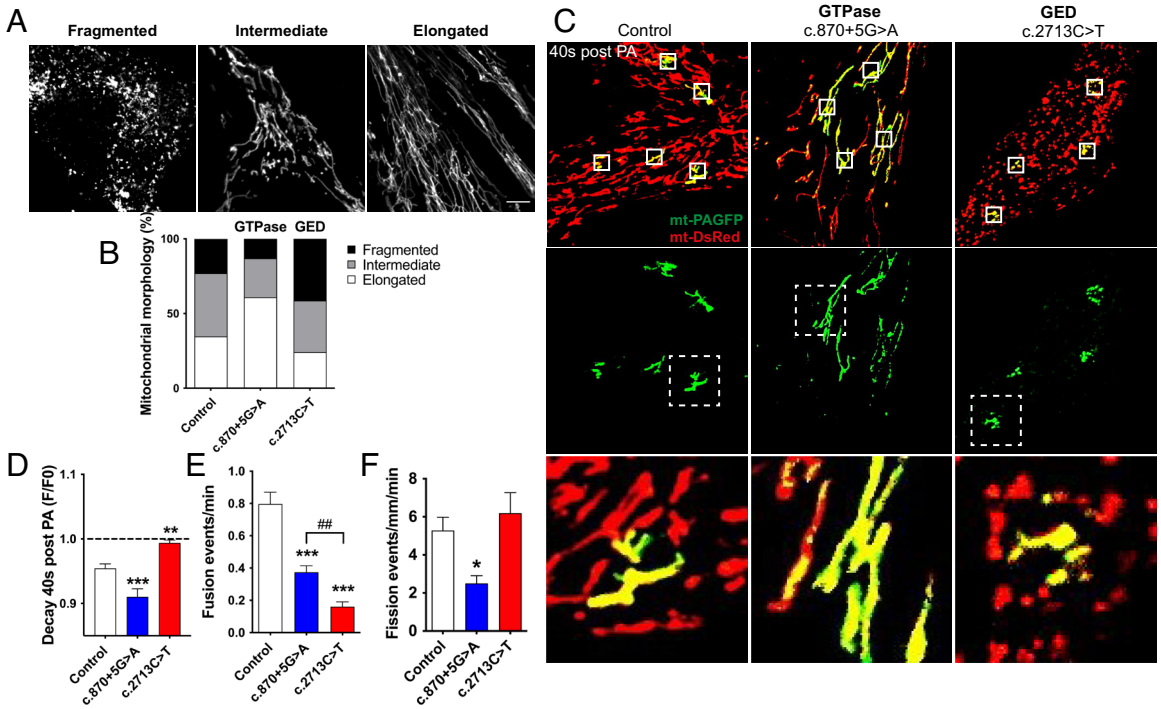

Fig. 3. GTPase and GED domain distinctly alter mitochondrial fusion/fission dynamics in ADOA patients-derived fibroblasts. (*A*) ADOA-derived fibroblasts coexpressing mt-PAGFP and mt-DsRed. Mitochondrial morphology was obtained using mt-DsRed by 560-nm laser excitation. Panels show representative images of the different mitochondrial morphologies observed (fragmented, intermediate, and elongated). (Scale bar, 10 μm.) (*B*) Quantification of mitochondrial morphology using mt-DsRed of control or ADOA-derived fibroblast carrying the mutants *OPA1*c.870+5G>A or *OPA1*c.2713C>T. (*C*) ADOA-derived fibroblast expressing mt-PAGFP and mt-DsRed 40 s after photoactivation of 5 × 5 μm ROIs (white squares) by 408-nm laser illumination, acquired upon 488- and 560-nm laser excitation; the *Bottom* panel shows *Inset* from the *Middle* panel, displaying one ROI highlighting the extent of mt-PAGFP diffusion. (*D*) Fluorescence decay quantification 40 s after mt-PAGFP photoactivation. (*E*) Fusion events frequency (control = 20 cells, *OPA1*c.870+5G>A = 22 cells, *OPA1*c.2713C>T = 24 cells; of ≥3 independent experiments). (*F*) Fission events frequency (control = 18 cells, *OPA1*c.870+5G>A = 17 cells, *OPA1*c.2713C>T = 17 cells; of ≥3 independent experiments). Data are mean ± SEM. **P* < 0.05, ***P* < 0.01, ****P* < 0,001 vs. control condition. ##*P* < 0.01 vs. c.870+G>A. Blue and red bars represent GTPase and GED mutants, respectively.

(cDNA) to generate the patient mutants and added c.899G>A and c.1334G>A for the GTPase domain and c.2708delTTAG for the GED domain (40, 41). The table in *SI Appendix*, Fig. S4 *A* and *B*, summarizes all the plasmids used in the following figures.

Profiles for mitochondrial dynamics proteins upon acute expression of GTPase and GED mutants. First, we confirmed by western blot that the WT OPA1 rescue in the *Opa1*$^{-/-}$ cells was comparable to the endogenous Opa1 from WT MEFs (*SI Appendix*, Fig, S5 *A* and *B*), as previously shown by us (26). Next, *Opa1*$^{-/-}$ cells were transfected with the *OPA1* c.870+5G>A or *OPA1* c.2713C>T plasmids. The GED mutant showed comparable expression levels with WT OPA1, while the GTPase mutant protein levels were considerably lower than the WT form (Fig. 4*A* and *SI Appendix*, Fig. S5*C*).

Acute expression of *OPA1* disease-causing mutants in an *Opa1*$^{-/-}$ background reproduced the instability of *OPA1*c.870+5G>A protein observed in the patient's cells. In *Opa1*$^{-/-}$, expression of the GED mutant showed downregulation of Mfn2 (Fig. 4*A* and *SI Appendix*, Fig. S5 *C–H*). Our results suggest that the overall changes observed in the patients are not induced solely by the mutants.

Because the patients' cells are heterozygous, where both mutant and WT OPA1 coexist, we also performed acute overexpression in WT MEFs. First, we found that the extent of OPA1 overexpression was 30% (*SI Appendix*, Fig. S5 *I* and *J*). Next, we tested whether the presence of OPA1 mutants alters the homeostasis of the WT form of OPA1 by acutely expressing *OPA1*c.870+5G>A or *OPA1*c.2713C>T. Fig. 4*B* and *SI Appendix*, Fig. S5*K* showed that upon mutants' expression, the GED mutant presented levels of overexpression comparable to *OPA1* WT, whereas the GTPase mutant showed no detectable overexpression, suggesting that the mutant form of the protein was unstable like it was in the patients and the *Opa1*$^{-/-}$ background. Also, upon *OPA1* overexpression, no detectable changes were found in the levels of Mfn1, Mfn2, Drp1, or its profission phosphorylated form pDrp1ser616 (Fig. 4*B* and *SI Appendix*, Fig. S5 *L–O*). The mitochondrial mass remained unchanged based on the Tomm20 abundance (Fig. 4*B* and *SI Appendix*, Fig. S5*P*).

Mitochondrial morphology and fusion dynamics upon acute expression of OPA1 mutants in Opa1*$^{-/-}$ *background. *Opa1*$^{-/-}$ MEFs were cotransfected with an OMM-targeted mCherry (mCherry-OMP25), mt-PAGFP, and OPA1 mutants. Based on the OMM-mCherry signal, *Opa1*$^{-/-}$ MEFs showed an entirely fragmented mitochondrial morphology (6). WT OPA1 partially rescued the mitochondrial network without causing elongation. The GTPase mutants exhibited no rescue, while only the GED mutant c.2713C>T showed partial normalization of mitochondrial morphology (*SI Appendix*, Fig. S6 *A* and *B*).

The fluorescence decay of mt-PAGFP showed that WT *OPA1* significantly rescued the mitochondrial continuity, whereas GTPase or GED mutants failed to do so (*SI Appendix*, Fig. S6 *A*, *C*, and *D*). Analysis of mitochondrial fusion activity revealed that in *Opa1*$^{-/-}$ cells, only *OPA1* WT and *OPA1*c.2713C>T restored fusion partially, to 40% compared to WT MEFs (*SI Appendix*, Fig. S6*E*). This result is in line with previously reported findings (25, 42), regarding the need for other isoforms of OPA1, in addition to isoform 1, to restore mitochondrial fusion activity fully.

The time resolution of our imaging setup (1 Hz) allowed us to determine the duration of the mitochondrial matrix fluorescent protein transfer during a fusion event as a measure of matrix mixing efficacy. In WT MEFs, mitochondrial matrix fusion was completed in 4.40 ± 0.31 s, and this was unaltered by the expression of WT *OPA1* or the GED mutant c.2713C>T; thus, when fusion is engaged, mitochondrial matrix mixing efficacy is not perturbed by the GED mutant (*SI Appendix*, Fig. S6*F*). Cells with acute expression of GTPase mutants showed no fusion events.

All in all, in an *Opa1* null background, acute expression of ADOA-*OPA1*-causing mutants does not support mitochondrial fusion activity. Only the GED mutant c.2713C>T caused partial rescue of mitochondrial fusion.

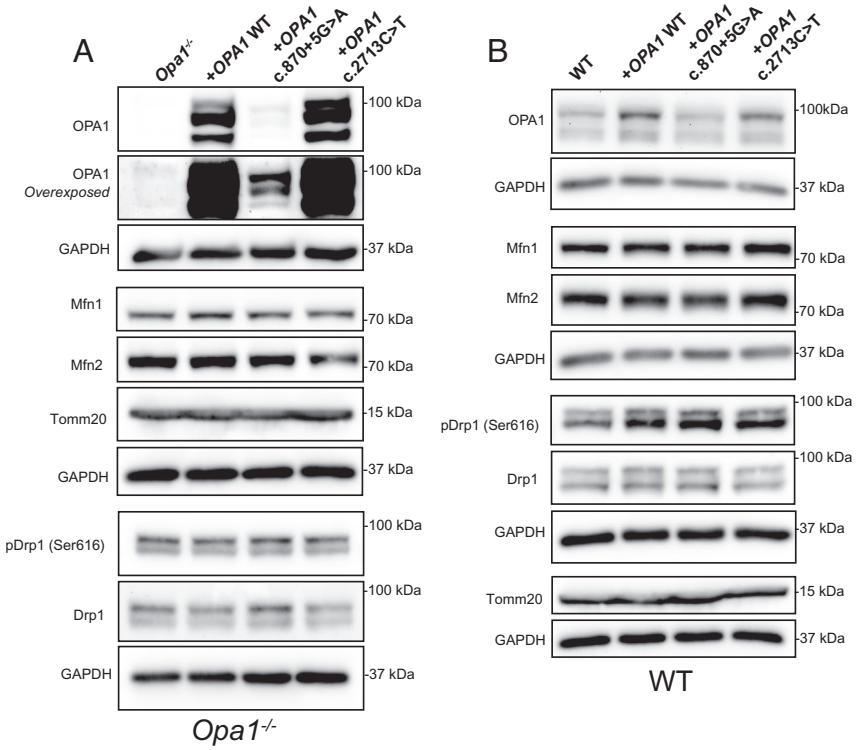

Fig. 4. Effect of OPA1 GTPase and GED domain-specific on mitochondrial dynamics proteins in *Opa1*$^{-/-}$ and WT MEFs. (*A* and *B*) *Opa1*$^{-/-}$ and WT MEFs were transfected with plasmids carrying the in vitro generated OPA1 ADOA mutants *OPA1*c.870+5G>A and *OPA1*c.2713C>T. Panels show representative western blot images of whole-cell extracts. *Left* and *Right* panels correspond to *Opa1*$^{-/-}$ cells rescued with *OPA1* mutants and WT cells overexpressing the *OPA1* mutants, respectively.

Mitochondrial form and fusion dynamics with acute and stable overexpression of OPA1 GTPase and GED mutants in WT background. First, we confirmed the extent of *OPA1* overexpression by qRT-PCR, and western blot, as previous reports showed that OPA1 overexpression leads to elongation, but excessive protein causes fragmentation (7). Our results showed that mRNA of all exogenous OPA1 WT and mutants were increased when compared with endogenous Opa1 mRNA (*SI Appendix*, Fig. S5*Q*). Also, we found no changes in endogenous Opa1 mRNA levels upon acute transfection with OPA1 mutants (*SI Appendix*, Fig. S5*R*). The abundance of all studied OPA1 mutants displayed comparable OPA1 levels to the WT OPA1 overexpression condition (*SI Appendix*, Fig. S5 *S* and *T*).

Mitochondrial morphology analysis showed that overexpression of WT *OPA1* or GTPase mutants *OPA1*c.870+5G>A and c.899G>A increased the percentage of cells with elongated mitochondria. In contrast, cells expressing the GTPase mutant *OPA1*c.1334G>A or GED mutants presented a higher frequency of cells with fragmented mitochondria (Fig. 5 *A* and *B*). Yet, morphological changes cannot be attributed to differences in DRP1 levels (*SI Appendix*, Fig. S5 *S* and *T*).

Mean decay kinetics of mt-PAGFP showed that *OPA1*c.870+5G>A and c.899G>A present prominent mitochondrial continuity, consistent with an elongated morphology. However, no beads-on-a-string phenotype was found in the GTPase-overexpressing WT MEFs. Opposite to the above results, GTPase mutant c.1334G>A and *OPA1* GED mutants displayed a discontinued mitochondrial phenotype, comparable to $Opa1^{-/-}$ cells (Fig. 5 *A*, *C*, and *D*). Notably, 20 s after photoactivation, cells expressing GED mutants *OPA1*c.2708delTTAG or c.2713C>T displayed no significant differences compared with the $Opa1^{-/-}$ cells, indicating that the coexistence of OPA1 carrying a truncated GED domain with the endogenous WT Opa1 (*SI Appendix*, Figs. S1*B* and S4*A*) interferes with the fusion activity, damaging mitochondrial continuity (Fig. 5 *A*, *C*, and *D*). Analysis of fusion activity showed that overexpression of WT *OPA1* increased the number of fusion events from 1.0 ± 0.2 events/min in the WT MEFs to 2.4 ± 0.2 events/min (Fig. 5*E*). However, all the mutant forms of OPA1 caused a significant decrease in the fusion activity, compared to WT cells (Fig. 5*E*).

The evaluation of the mitochondrial matrix mixing kinetics also revealed that overexpression of *OPA1* WT does not affect the matrix mixing efficacy during mitochondrial fusion. Strikingly, *OPA1* GTPase and GED mutants increased the duration of matrix proteins mixing during fusion events completion, suggesting that the presence of the mutants might alter the docking and mixing of IMM during fusion pore opening and subsequent matrix proteins mixing (Fig. 5*F*).

Finally, we created WT cells stably overexpressing OPA1 WT, c.870+5G>A, and c.2713C>T. Mitochondrial morphology analysis showed that cells carrying and overexpression of OPA1 WT and the GTPase mutant c.870+5G>A increase the proportion of cells with an elongated network (Fig. 5*G* and *SI Appendix*, Fig. S5*U*). Also, cells overexpressing the GED mutant OPA1c.2713C>T displayed more cells with a fragmented network (Fig. 5*G* and *SI Appendix*, Fig. S5*U*).

Altogether, these results are consistent with those found in the ADOA-derived fibroblasts. The presence of *OPA1*c.870+5G>A displayed a more continuous mitochondrial network in both acute and stable overexpression, despite the low expression levels of OPA1 and a decrease in the mitochondrial fusion rate (Fig. 4*B* and *SI Appendix*, Fig. S5*K*) in the WT background, as observed in ADOA-derived fibroblasts (Fig. 3 *D*–*F*). This effect may be explained by the inhibition of fission observed in patients' cells (Fig. 3*F*). Also, the mutant *OPA1*c.899G>A shared this phenotype, mounting evidence that some, but not all, GTPase *OPA1* mutants induce a more complex disruption of mitochondrial fusion–fission balance in the severe presentation of the disease. In addition, the acute or stable overexpression of *OPA1*c.2713C>T in the WT cells recapitulated the effect shown in the ADOA-derived fibroblasts, involving mitochondrial fragmentation and fusion inhibition (Fig. 3 *D* and *E*). Yet, further research will be needed to understand how specific mutations of *OPA1* interfere with fission signaling.

Mechanistic Studies.

GED region is expendable for OMM–IMM fusion coupling and OPA1 oligomerization but necessary for GTPase activity. We evaluated the fusion mixing kinetics using a cell fusion assay of two different cell populations expressing an OMM-targeted mCherry (mCherry-OMP25) and an IMM-targeted GFP (COXIV8aGFP), while improved space–time resolution was achieved by live cell imaging using Airyscan detection. Upon Polyethylene glycol-induced cell fusion, we detected individual fusion events between an mCherry-OMP25-expressing mitochondrion and a COXIV8aGFP-expressing one (Fig. 6*A* and Movie S2). This approach informed the temporal aspects of the sequential OMM and IMM mixing (Fig. 6 *B* and *C*). In WT MEFs, mCherry-OMP25 equilibration upon fusion was completed in 14.4 ± 1.2 s, whereas in $Opa1^{-/-}$MEFs rescued with WT *OPA1* or the GED mutant, *OPA1*c.2713C>T, it was completed in approximately 10 s (Fig. 6*D*). As to IMM fusion, in WT cells, COXIV8aGFP equilibration was reached in 13.0 ± 1.2 s; however, in rescued $Opa1^{-/-}$cells expressing *OPA1* WT or GED mutant *OPA1*c.2713C>T, IMM mixing was completed in nearly 7 s (Fig. 6*E*). In Fig. 5*E*, we showed that the GTPase mutants present no fusogenic activity; consistently, no OMM and IMM fusion was detected when expressing *OPA1*c.870+5G>A. To study whether there is a perturbation of OMM and IMM sequential fusion coupling, we measured the gap between the starting time point between OMM and IMM fusion. However, no significant differences were found in the three conditions that showed fusion events (*SI Appendix*, Fig. S7*A*). Therefore, maintaining OMM and IMM fusion mixing kinetics by GED mutant may contribute to a less severe form of ADOA.

To explore other OPA1 functions that could be linked to ADOA-causing mutants, we tested OPA1 oligomerization, given its role in cristae junction tightening (20). $Opa1^{-/-}$cell extracts were treated with the chemical cross-linker BMH to test the homotypic oligomerization of OPA1. Our data showed that exogenous OPA1 WT could form oligomers (*SI Appendix*, Fig. S7 *B* and *C*), consistent with previously reported data (20, 42). Interestingly, enhanced oligomerization of OPA1 was observed for GED mutant c.2713c>t *OPA1*. Thus, these data suggest that the GED domain is not required for homotypic OPA1 oligomerization. The GTPase mutant *OPA1*c.870+5G>A showed no oligomers (*SI Appendix*, Fig. S7 *B* and *C*). To test whether the absence of oligomers resulted from the mutation in the GTPase domain or its low expression, we tested two other mutants: the GTPase point mutation *OPA1*c.1334G>A and the GED mutant *OPA1*c.2818+5G>A carrying a splicing defect (*SI Appendix*, Fig. S7*D*). Although both mutants were detected, the GED mutant *OPA1*c.2818+5G>A showed lower levels than the GTPase point mutation *OPA1*c.1334G>A. Yet, we detected the presence of OPA1 oligomers with each mutant, suggesting that the low expression levels for the GTPase mutant *OPA1*c.870+5G>A likely hindered the visualization of oligomers (*SI Appendix*, Fig. S7 *B* and *C*).

Also, the presence of oligomers in the GED mutant *OPA1*c.2818+5G>A confirmed that the GED domain is not required for homotypic OPA1 oligomerization (*SI Appendix*, Fig. S7*D*). This was an unexpected finding, considering that the

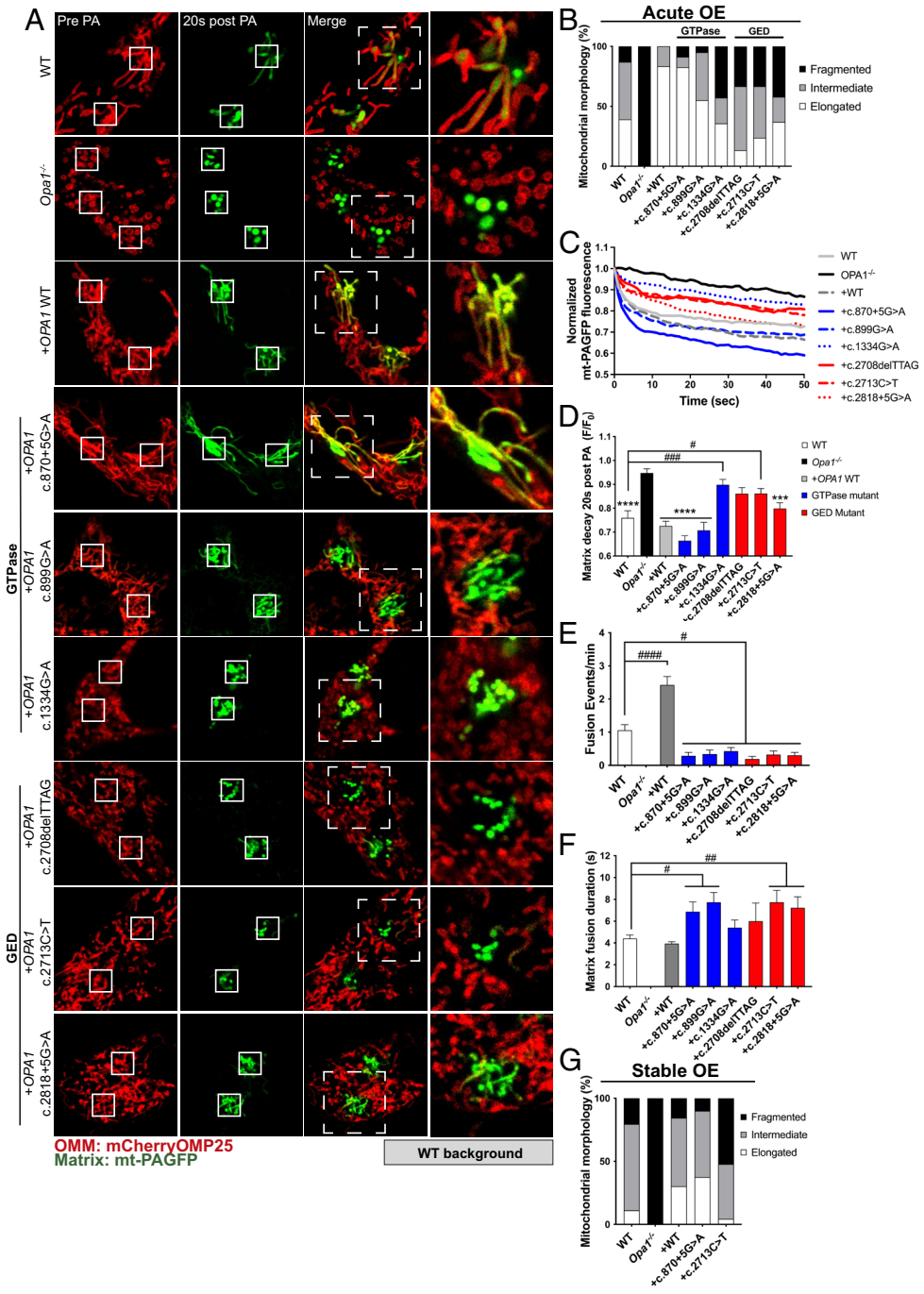

Fig. 5. Expression of *OPA1* GTPase and GED domain-specific mutants differentially disrupts mitochondrial fusion dynamics in WT MEFs. (*A*) Cells acutely coexpressing OMM-targeting mCherry-OMP25, mt-PAGFP, and OPA1 mutants. Each row displays experiments before and 20 s after photoactivation of 3 × 3 µm ROIs (white squares) by two-photon laser illumination (760 nm), acquired upon 488- and 560-nm laser excitation; the *Right* panel shows *Inset* from the *Middle* panel, displaying one ROI (white dashed square) highlighting the extent of mt-PAGFP diffusion. (*B*) Quantification of mitochondrial network morphology of WT MEFs acutely overexpressing *OPA1* mutants classified as elongated, intermediate, and fragmented. Data are at least 15 cells per condition from ≥3 independent experiments (WT = 23 cells, *Opa1*$^{-/-}$ = 24 cells, WT+*OPA1*WT = 33 cells, WT+*OPA1*c.870+5G>A = 23 cells, WT+*OPA1*c.899G>A = 20 cells, WT+*OPA1*c.1334G>A = 20 cells, WT+*OPA1*c.2708delTTAG = 15 cells, WT+*OPA1*c.2713C>T = 21 cells, WT+*OPA1*c.2818+5G>A = 19 cells. (*C*) Quantification of mt-PAGFP decay after photoactivation. Lanes are means of individual ROIs. (*D*) The bar chart displays the mt-PAGFP fluorescence decay 20 s after PA. Data are mean ± SEM of cells used in *B*. (*E*) Mitochondrial fusion events frequency. Bar charts show mean ± SEM of the same cells used in *B*. (*F*) Quantification of mitochondrial fusion duration (time to completion of mt-PAGFP transference from a donor to an acceptor mitochondrion). Bar charts show mean ± SEM of the same cells used in *B*. (*G*) Mitochondrial morphology quantification on WT MEFs stably overexpressing OPA1 WT, OPA1 c.870+5G>A, or OPA1 c.2713C>T. Data are mean ± SEM. ***P < 0.001, ****P < 0.0001 vs. *Opa1*$^{-/-}$. #P < 0.05, ##P < 0.01, ###P < 0.001, ####P < 0.0001 vs. WT. Blue and red bars represent GTPase and GED mutants, respectively.

WT GED domain forms a coiled-coil conformation (*SI Appendix*, Fig. S8), as determined in silico by the bioinformatics tool DeepCoil (43). This analysis revealed that coiled-coil domain 2 was lost in *OPA1*c.2713C>T but not in *OPA1*c.2818+5G>A (*SI Appendix*, Fig. S8). Thus, our data underline that although the GED OPA1 region has a protein–protein interaction potential, as previously reported (44), it is not relevant for OPA1 homotypic oligomer formation.

Next, we evaluated the oligomerization of OPA1 mutants in the context of endogenous Opa1. WT MEFs were transfected with the *OPA1* mutants. Opa1 complexes were clearly defined, with no significant changes in abundance, except for the *OPA1*c.2713C>T

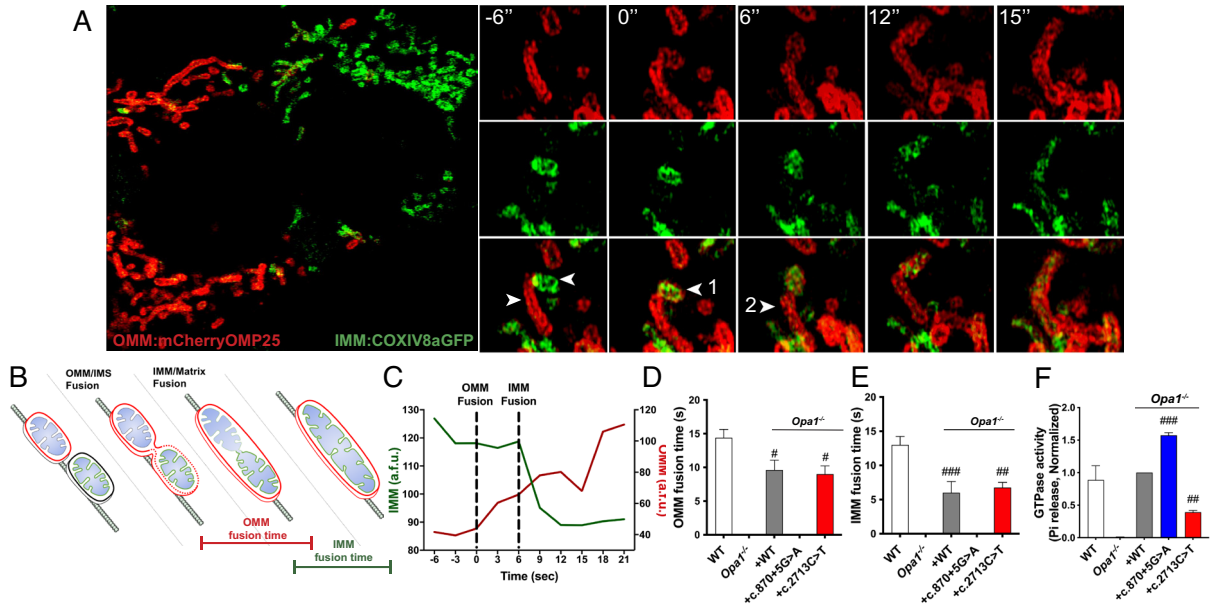

Fig. 6. Role of the OPA1 GED region in OMM–IMM fusion kinetics, OPA1 oligomerization, and GTPase activity. (*A*) Left panel: Representative example of a cell fusion assay of cells expressing mCherry-OMP25 (OMM) and COXIV8aGFP (IMM). Right panel: inset from left panel highlighting a sequential OMM and IMM fusion event. Live cell imaging was conducted at an LSM880 Zeiss confocal with Airyscan detectors. (*B*) Schematic representation of OMM, followed by IMM fusion, between two adjacent mitochondria. (*C*) Sequential OMM and IMM fusion mixing kinetics of mitochondrial fusion event indicated in white arrows in panel *A*. (*D*) OMM mixing completion time in *Opa1*$^{-/-}$ MEFs expressing *OPA1* mutants (WT = 10 fusion events, *Opa1*$^{-/-}$ +*OPA1* WT = 5 fusion events, *Opa1*$^{-/-}$ +*OPA1* c.2713C>T = 4 fusion events). Bar charts show mean ± SEM. (*E*) IMM mixing completion time in *Opa1*$^{-/-}$ MEFs expressing *OPA1* mutants. Bar charts show mean ± SEM. (*F*) GTPase activity assay measured in immunopurified proteins by malachite green assay. n = 3. Data are mean ± SEM. #*P* < 0.05, ##*P* < 0.01, ###*P* < 0.001 vs. WT. Blue and red bars represent GTPase and GED mutants, respectively.

mutants that tended to increase the presence of oligomers (*SI Appendix*, Fig. S7 *E* and *F*). This observation is consistent with the data described in the *Opa1*$^{-/-}$ background, suggesting that GED may act as a regulator of OPA1 oligomerization.

Given the changes in Mic60 and Mic19 levels detected in patient cells and that OPA1 interacts with the MICOS complex to stabilize the cristae junction (45), we measured Mic60 and Mic19 in *Opa1*$^{-/-}$ cells expressing OPA1 mutants. Conversely to patient cells (Fig. 1 *A* and *B*), the acute expression of OPA1 and ADOA-causing mutants in the *Opa1*$^{-/-}$ or WT background involved no consequences for Mic60 and Mic19 protein levels and Mic60 oligomerization (*SI Appendix*, Fig. S7 *G–L*), suggesting that the chronic presence of the mutants may account for our observations of changes of the MICOS in the patients' cells.

Considering the absence of experimental data about the role of OPA1's GED on the protein's GTPase activity, we immunopurified OPA1 from transfected *Opa1*$^{-/-}$ cells and tested the GTPase activity as previously described (46, 47). Our results showed that the overexpressed OPA1 WT exhibited GTPase activity comparable with the endogenous Opa1 from WT MEFs (Fig. 6*F*). The GTPase mutant *OPA1*c.870+5G>A displayed significantly enhanced GTPase activity, suggesting that this mutation produces a constitutively active-like protein. In addition, the GED mutant *OPA1*c.2713C>T exhibited a decrease in the GTPase activity (Fig. 6*F*), uncovering that this domain is required for proper GTPase activity, as previously suggested (22).

Overall, our data indicate that the absence of the GED region does not alter the kinetics of OMM and IMM fusion execution. GTPase and GED domains are dispensable for OPA1 oligomer formation, despite the coiled-coil nature of GED. In addition, the GED region of OPA1 is expendable for Opa1 or Mic60 oligomer formation, suggesting no major role in cristae junction stabilization. However, it plays a role in the GTPase activity of the protein, providing a mechanistic explanation for the role of GED in mitochondrial fusion execution.

Proteostasis of OPA1 ADOA-causing mutants. Given the role of mitochondrial membrane potential in protein import and OPA1 processing from long to short forms (48), we explored whether OPA1 mutants alter the processing of OPA1. To test the depolarization-induced processing, *Opa1*$^{-/-}$ cells transfected with WT or mutant forms of *OPA1* were treated with a mitochondrial uncoupler, FCCP. Fig. 7*A* shows that endogenous Opa1 in WT MEFs and exogenous OPA1 in the *Opa1*$^{-/-}$ background exhibited processing of isoform 1 from the long into the short form (Fig. 7 *A* and *B*). The same was observed with the GED mutant *OPA1*c.2713C>T. However, the GTPase mutant *OPA1*c.870+5G>A revealed low resting levels of the short form, and after the FCCP treatment, there was no processing. Furthermore, there was an accumulation of *OPA1*c.870+5G>A preprotein (Fig. 7 *A* and *B*). To measure OPA1 import to mitochondria, we calculated the ratio of total OPA1 relative to the levels of the preprotein form. *OPA1*c.870+5G>A quickly decreased the imported protein upon FCCP stimulation (Fig. 7*C*). These data indicate that mitochondrial import and processing are impaired for the GTPase mutant *OPA1*c.870+5G>A.

To further understand the mechanism involved in low protein levels of the *OPA1*c.870+5G>A mutant, cycloheximide (CHX) was used to stop the mRNA translation and characterize the protein's stability. After CHX treatment, we observed a reduction in the preprotein band of OPA1 WT and GED mutant *OPA1*c.2713C>T; however, the total protein remained stable 6 h after the translation was stopped (Fig. 7 *D* and *F* and *SI Appendix*, Fig. S7*M*). By contrast, the GTPase mutant *OPA1*c.870+5G>A showed a reduction in the preprotein and a rapid decrease in the total protein levels after the translation was stopped, indicating a short half-life of this mutant (Fig. 7 *D* and *F* and *SI Appendix*, Fig. S7*M*).

To evaluate whether this result is a consequence of the GTPase mutation or an outcome of misfolding due to the splicing defect, we studied two other mutants: a point mutation in the GTPase domain, *OPA1*c.1334G>A, and a GED domain mutant, containing a splice

defect *OPA1*c.2818+5G>A. The experiments revealed that mutants containing a splice defect are rapidly degraded after translation (Fig. 7 *E* and *F*). Next, as the splicing defect mutants exhibited a very short half-life, we used the proteasome inhibitor MG132 to test whether the misfolded proteins were being degraded by the ubiquitin–proteasome system (UPS), as previously described for IMM proteins (49). The accumulation of endogenous Opa1 or the exogenous OPA1 was relatively low (Fig. 7 *G–I* and *SI Appendix*, Fig. S7*N*) as well as for mutants carrying point mutations *OPA1*c.1334G>A and *OPA1*c.2713C>T (Fig. 7 *G–I* and *SI Appendix*, Fig. S7*N*). Furthermore, among mutants carrying splicing defects, the GTPase mutant *OPA1*c.870+5G>A showed considerable accumulation upon proteasome inhibition, yet the accumulation of GED mutant *OPA1*c.2818+5G>A was milder. Finally, none of the mutants are apparently degraded by autophagy/mitophagy since changes in the mitochondrial mass markers or the autophagy marker LC3I/LC3II were undetected (*SI Appendix*, Fig. S7 *O* and *P*). Thus, our data show that *OPA1*c.870+5G>A displays very low protein levels because the translated protein is degraded by the UPS, uncovering a haploinsufficiency-like phenotype.

Discussion

By combining the study of patient-derived cells with acute and stable rescue overexpression paradigms, we were able to establish mitochondrial ultrastructure and dynamics patterns for both *OPA1* GTPase and GED mutations (Fig. 8). Ultrastructural and morphological defects were observed in all studied mutants, accompanied by distinct aberrations in cristae abundance and cristae characteristics, uncovering perturbations in cristae maintenance. By contrast, we found domain-specific differences in mitochondrial fusion and MICOS protein levels. Our findings suggest that the GTPase mutants induce mitochondrial fusion–fission misbalance, whereas GED mutants involved defects confined to fusion. Three out of four *OPA1* mutations we studied led to haploinsufficiency in patients' cells. Additional work is needed to explain how these different effects on mitochondrial dynamics impact the clinical severity and tissue specificity seen in patients with ADOA.

ADOA-derived fibroblasts displayed distinct mitochondrial dynamics protein profiles; those with low protein levels of OPA1 also showed low levels of MIC60 (Fig. 1 *A* and *B*). OPA1 and MIC60 can physically interact (21, 45), support cristae biogenesis (45), and participate in OMM–IMM interaction dynamics (50). Acute expression of OPA1 mutants exhibited no effect on MICOS protein levels in the *Opa1* null and WT background (*SI Appendix*, Fig. S7); thus, the codownregulation of OPA1 and MIC60 observed in the patient-derived cells may be a consequence of long-term adaptations. Cells bearing GTPase mutants c.870+5G>A and c.889C>T displayed a loss of cristae junction with normal cristae lumen width. Moreover, they exhibited cristae discontinuities with partial swelling, suggesting that low levels of OPA1 and MIC60, in the context of *OPA1* mutants, are sufficient to support cristae formation but not long-lasting maintenance of cristae junction. Others have shown that expression of an *OPA1* mutant with GTPase and fusion-defective activity, Q297V (42), and G300E (c.899G>A) (25), partly or poorly recover cristae ultrastructure, respectively; however, these studies do not show quantitative characteristics of the cristae junction.

Our data show that *OPA1*c.870+5G>A acts as a constitutively active GTPase; nonetheless, it is rapidly degraded after translation, evoking a haploinsufficiency-like phenotype. Also, the increased GTPase activity is not enough to compensate for the low protein levels to support fusion likely because of protein folding and dimerization impairment due to the loss of exon 8, which is critical for

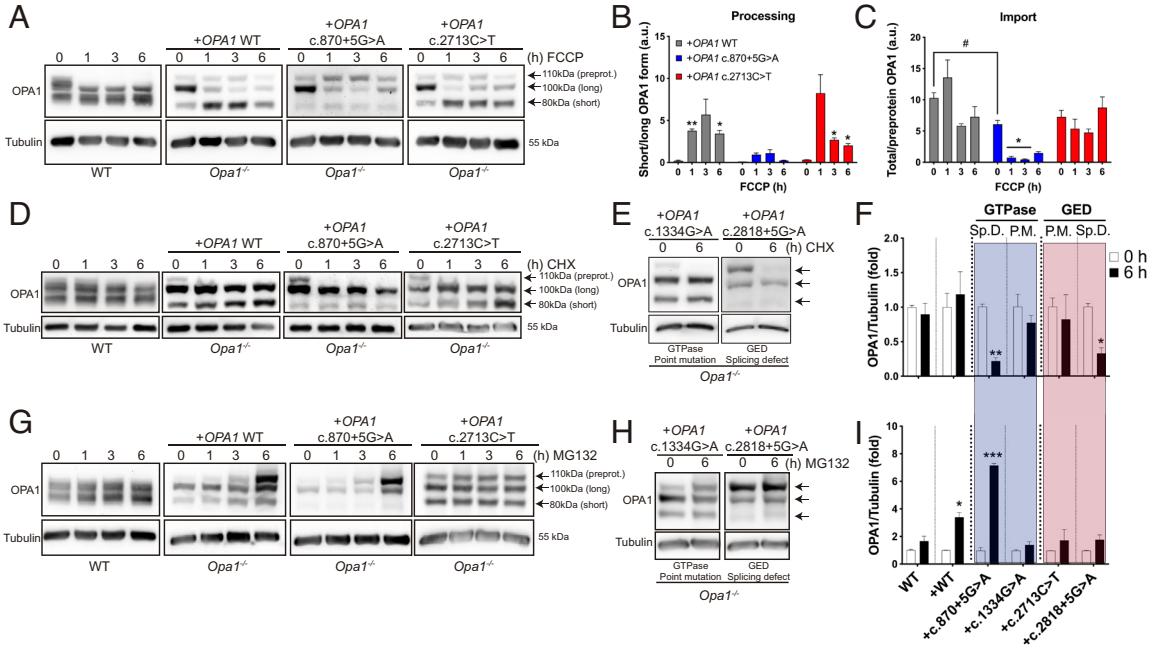

Fig. 7. OPA1 GTPase and GED mutant protein stability. (*A*) WT and *Opa1*$^{-/-}$ MEFs expressing *OPA1* GTPase c.870+5G>A or GED c.2713C>T mutants were incubated with FCCP 1 μM for 1, 3, and 6 h, representative OPA1 western blots of whole-cell extracts. (*B*) OPA1 processing was quantified as the ratio of the OPA1 short form vs. the OPA1 long form. n = 3. (*C*) OPA1 importation was quantified as OPA1 total (long + short form)/OPA1 preprotein. (*D*) WT and *Opa1*$^{-/-}$ MEFs expressing *OPA1* GTPase or GED mutant were incubated with 50 μM of cycloheximide (CHX) for 1, 3, and 6 h, representative OPA1 western blots. (*E*) OPA1 protein levels in cells expressing a GTPase point mutation (P.M.) or a GED splice defect (Sp.D.), upon incubation with CHX for 6 h. (*F*) The bar plot shows western blot quantification of WT or *Opa1*$^{-/-}$ MEFs expressing Sp.D. or P.M. mutants for the GTPase domain or GE region after incubation with CHX for 6 h. n = 3. (*G*) WT and *Opa1*$^{-/-}$ MEFs expressing *OPA1* GTPase c.870+5G>A or *OPA1* GED c.2713C>T mutants were incubated with 25 μM of MG132 to determine the ubiquitin–proteasome system role in OPA1 protein levels. (*H*) Cells expressing a GTPase P.M. or a GED Sp.D. were incubated with MG132 for 6 h, to test OPA1 protein levels by western blot. (*I*) Western blot quantification of WT or *Opa1*$^{-/-}$ MEFs expressing splicing Sp.D. or P.M. for GTPase domain or GE domain after incubation with MG132 for 6 h. n = 3. Data are mean ± SEM *P < 0.05, **P < 0.01, ***P < 0.001 vs. t0. #P < 0.05 vs. *Opa1*$^{-/-}$ *+OPA1* WT t0. Blue and red bars represent GTPase and GED mutants, respectively.

GTPase activity (51). Interestingly, the scarce presence of this mutant in the context of the WT *OPA1* allele, both in the patient-derived cells and in WT MEFs, led to elongated mitochondrial morphology but inhibited mitochondrial fusion activity; these features were also shared by Opa1 WT cells expressing *OPA1*c.899G>A. In addition, the patient's fibroblasts bearing c.870+5G>A *OPA1* exhibited a beads-on-a-string phenotype due to an imbalance in the execution of fission. Incomplete mitochondrial constriction has been described during acute ablation of *OPA1* (52), linked to mitochondrial depolarization in a *Drp1* null background (53), and as part of a fission-priming process (50). Moreover, short forms of Opa1 lead to fragmented mitochondria and are proposed to be linked to mitochondrial fission (48). In contrast, depletion of OPA1 increases DRP1 cellular levels (54), and fusion and fission machinery coincide at endoplasmic reticulum contact points to execute both processes (55). This study reports elongated mitochondria induced by an ADOA *OPA1* mutant, such as *OPA1*c.870+5G>A and c.899G>A, whereas c.1334G>A induces fragmentation and fusion inhibition. Yet, DRP1 levels were unaltered in the patient cells; thus, further studies are needed to understand the underlying mechanisms. These results suggest that some GTPase mutants involve dysregulation of fusion and fission, with fission being likely more prominent, whereas GED mutants involve defects exclusive to mitochondrial fusion dynamics.

We showed that *OPA1*c.870+5G>A protein product processing is not triggered upon mitochondrial membrane potential dissipation. Possibly, the scarce protein product of this exon-skipping mutant may be either interfering with its processing domain, S1, or else perturbing the access of proteases to the processing domains of WT forms of OPA1. Furthermore, the c.870+5G>A OPA1 protein product lacks oligomerization, which might be due to its low abundance or to the close localization of the mutation to the coiled-coil 1 domain, which is predicted to homopolymerize OPA1 (14).

OPA1 GED mutants c.2713C>T and c.2818+5G>A exhibited dissimilar OPA1 levels, likely because the latter mutant causes a splicing defect and is rapidly degraded. Still, both mutants showed comparable ultrastructure phenotypes, with swollen mitochondria, short cristae, and increased cristae junction and lumen width. Yet, acute expression of GED mutant c.2713C>T in an $Opa1^{-/-}$ background exhibited enhanced OPA1 self-assembly; however, $OPA1^{R905*}$ (c.2713C>T) did not prevent cell death induced by intrinsic stimuli in WT MEFs background (20), suggesting that other mechanism may be involved in the regulation of the cristae junction.

*OPA1*c.2713C>T is our study's only mutant that could partially restore mitochondrial fusion in $Opa1^{-/-}$cells. Despite its low GTPase activity, it did not differ from OPA1 WT in OMM and IMM fusion duration. Here, we confirmed that the OPA1 GED region supports GTPase activity, as in the dynamin's family (12) and Dmn1p (56). Interestingly, IMM fusion can proceed by heterotypic interaction between OPA1 and cardiolipin (19). In dynamins, GED coexists with the Pleckstrin homology domain (PH), which helps to bind lipids (57). Recent structural analysis of a putative PH domain in OPA1, particularly an exon 25-encoded peptide, exhibits a higher isoelectric point than GED, encoded by exons 26-29. The exon 25-encoded peptide, which is a positively charged domain close to GED, could help OPA1 interact with negatively charged phospholipids, such as cardiolipin (58). Also, crystal structure analysis of the OPA1 orthologue Mgm1 (*Chaetomium thermophilum*) identified a lipid-binding domain referred to as "paddle," comparable to the PH-like domain in dynamin protein (59). Our approach confirms that OPA1 minus the GED region is sufficient to support mitochondrial fusion; however, whether this is based on homotypic or heterotypic interaction requires further studies. In addition, based on *OPA1*c.2713C>T-enhanced oligomerization and despite the absence of a predicted coiled-coil domain predicted in the GED region, our data suggest that OPA1 oligomer formation relies on coiled-coil one domain. This protein–protein interaction may determine both homotypic IMM fusion and cristae maintenance.

In contrast to the partial fusion activity of *OPA1*c.2713C>T in $Opa1^{-/-}$ MEFs, acute expression of all GED mutants that we studied in WT MEFs and ADOA-derived cells induced mitochondrial fragmentation and abolished mitochondrial fusion, suggesting that GED-located mutants are likely to play a dominant-negative role in the context of the OPA1 WT form. Overall, different pieces of evidence show that OPA1 mutants lead to mitochondrial fragmentation, independent of the localization of the genetic defect in the *OPA1* gene (25, 40, 60, 61). Our data on the acute expression of *OPA1*c.2708delTTAG (Δ58) contradict the findings by Olichon et al. (40) in HeLa cells. Still, they are in keeping with mitochondrial fragmentation previously shown by us upon acute expression of OPA1 Δ58 in adult skeletal muscle (62).

Regarding OMM and IMM mixing kinetics, we showed that expression of both WT *OPA1* and *OPA1*c.2713C>T displays faster mixing kinetics compared with mitochondria in WT MEFs, suggesting that human OPA1 might be more efficient than the murine form of Opa1 in executing IMM fusion or that additional OPA1 isoforms contribute to slower execution of OMM and IMM fusion and, consequently, protein content mixing. Also, given that bilayer fluidity relies on phospholipid composition (63), the observed differences may also be explained by differences in mitochondrial lipid composition in $Opa1^{-/-}$ vs. WT MEFs, as recently reported (64).

Concerning the proteostatic balance of OPA1 splicing defect mutants, our data showed that UPS rapidly and distinctly degraded *OPA1*c.870+5G>A protein. UPS-mediated degradation has also been demonstrated for a pathogenic mitochondrial protein containing an exon deletion (65). Degradation of *OPA1*c.2818+5G>A protein might be mediated by IMM proteases involved in protein quality control (66).

Finally, over 250 OPA1 variants cause ADOA, and the same variant can cause isolated optic atrophy or ADOA plus in individuals of the same family. Thus, it is difficult to establish a tight genotype–phenotype correlation. Yet, the analysis of multiple patients with mutations in the GTPase domain is associated with more severity (30). Our study correlated genotype to mitochondrial dynamics phenotype, but the genetic background variability and environmental factors may determine ADOA's severity.

Materials and Methods

ADOA Patients-Derived Cells and MEFs. Experiments were performed in fibroblasts derived from ADOA patients and control individuals or mouse embryonic fibroblasts (MEFs). Patient-derived cells were provided by Newcastle Research Biobank for Rare and Neuromuscular Diseases, based on a Material Transference Agreement with Pontificia Universidad Católica de Chile. Cells were cultured as described in *SI Appendix, Materials and Methods*.

Mitochondrial Dynamics Studies by Confocal Microscopy. Mitochondrial matrix fusion or fission dynamics of ADOA-derived fibroblast were studied using a laser-scanning microscope Nikon Eclipse C2, using a 63×/1.4 ApoPlan objective, located at Advanced Microscopy Facility, Pontificia Universidad Católica de Chile. In MEFs, experiments were performed using a laser-scanning microscope system (63×/1.4 NA, Laser Scanning Microscope (LSM) 780 Non-Linear Optics (NLO) with Gallium Arsenide phosphide (GASP) detectors; Carl Zeiss) located at the MitoCare Center at Thomas Jefferson University. Experiments and analysis are described in detail in *SI Appendix, Materials and Methods*.

OMM and IMM Fusion Dynamics Studies by Cell Fusion Assay. WT or $Opa1^{-/-}$ MEFs exogenously expressing *OPA1* WT or domain-specific mutant constructs and the IMM-targeted protein COXIV8a-GFP or the OMM-targeted protein mCherry-OMP25. After 24 h, the cells were plated and cocultured for 24 h at high

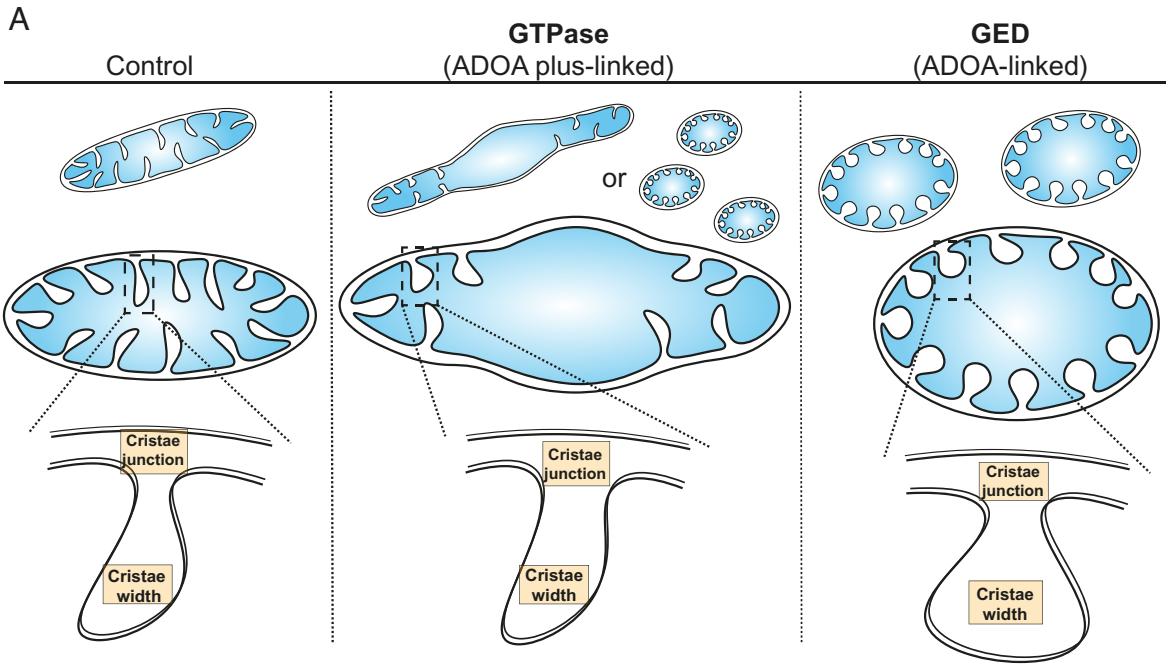

B

		GTPase	GED
Patients	Mutants	c.870+5G>A / 889C>T	c.2713C>T / 2818+5G>A
	Ultrastructure	Larger area / Interrupted cristae	Larger area / Swollen mito
	Cristae junction	Open	Open
	Cristae width	–	Wider
	Morphology	Hyperelongated / n.e.	Fragmented / n.e.
	Fusion activity	Inhibited / n.e.	Inhibited / n.e.
WT background	Mutants	c.870+5G>A / 899G>A / 1334G>A	c.2708delTTAG / 2713C>T / 2818+5G>A
	Morphology	Hyperelongated / Fragmented	Fragmented
	Fusion activity	Inhibited	Inhibited
	Fusion duration	Up	Up
Opa1 KO background	Mutants	c.870+5G>A / 899G>A / 1334G>A	c.2708delTTAG / 2713C>T / 2818+5G>A
	Morphology	Fragmented	Fragmented / Partially rescued / Fragmented
	Fusion activity	Zero	Zero / Rescued / Zero
	Fusion duration	No fusion	No fusion / Rescued / No fusion
	Oligomerization	Zero / n.e. / –	n.e. / Up / –
	GTPase activity	Up / Down[a] / Down[a]	n.e. / Down / n.e.

Fig. 8. Distinctive mitochondrial fusion dynamics and ultrastructure defects in OPA1 domain-specific mutants; summary of main findings. (*A*) Scheme of main common features for the OPA1 GTPase and GED ADOA-causing mutants studied in this work. The cartoon shows that *OPA1* GTPase ADOA plus–causing mutants exhibit dissimilar mitochondrial morphology (elongated or fragmented), cristae discontinuities, and cristae junction loss. *OPA1* GED ADOA-causing mutants exhibited fragmented mitochondria, swollen organelles, loss of cristae junction, and wider cristae lumen. (*B*) Table summarizing the domain-specific findings in ADOA patient-derived cells and acute expression of ADOA-causing mutants in a WT and Opa1 KO background. –, unchanged compared to the control condition; n.e., not evaluated. [a]Data obtained from ref. 46.

confluency. The cells were pretreated with CHX 50 µm for 30 min and then washed three times with Phosphate buffer saline (PBS) and incubated for 60 s with a solution of Dulbecco's modified Eagle Medium (DMEM) without Fetal bovine serum (FBS) and PEG1500 50%. The PEG solution was removed by washing extensively with DMEM without FBS. The cells were kept in DMEM + 10%FBS CHX for 30 min and analyzed by confocal microscopy. Mitochondrial OMM and IMM fusion assays in MEFs were performed in a confocal microscope Zeiss 880 equipped with an Airyscan detector. The 488 and 560 nm laser lines were used for times series of and z-stack. The images were recorded in five slices every 3 s for 6 min.

Data, Materials, and Software Availability. Western blot data have been deposited in the Open Science Framework and can be found at https://osf.io/ejp7t/?view_only=e23eb621818540a99d7b5ed304a4e7f7 (67).

ACKNOWLEDGMENTS. We thank David Weaver, Alejandro Munizaga, and Ximena Vergés for their valuable technical support. We also thank Guy Lenaers for the plasmid backbone encoding OPA1 (pCCEY) plasmids and helpful discussion, Heidi McBride, Erin Seifert, György Csordás, Esteban Jorquera, Janine Santos, and María Paz Marzolo for valuable discussion. We thank Enrique Brandan for his help with reagents. Finally, we thank all former and current lab members for their fruitful discussion. The Chilean Government supported this work through Agencia Nacional de Investigación y Desarrollo (ANID) PhD fellowship 21181402 to B.C.-S., Vicerrectoria de Investigación Pontificia Universidad Católica de Chile (VRI-UC) PhD fellowship to B.C.-S., ANID PhD fellowship 21191304 to D.L., ANID PhD fellowship 21211363 to J.M., ANID PhD fellowship 21150971 to D.A., FONDECYT grant 1171004 to M.K.S.-H., FONDECYT grant 1191151 to M.E.A. R.H. is supported by the Newton Fund (MR/N027302/1), the Medical Research Council (UK) (MR/N025431/1), the Wellcome Investigator Award (109915/Z/15/Z), the Lily Foundation UK, and the Evelyn Trust. R.H. is a member of the European Reference Network for the thematic grouping of rare Neuromuscular Diseases (EURO-NMD). P.Y.-W.-M. is supported by an Advanced Fellowship Award (NIHR301696) from the UK NIH Research (NIHR) and by a Clinician Scientist Fellowship Award (G1002570) from the Medical Research Council (United Kingdom) and also receives funding from Fight for Sight (United Kingdom), the Isaac Newton Trust (United Kingdom), Moorfields Eye Charity, the Addenbrooke's Charitable Trust, the National Eye Research Centre (United Kingdom), the International Foundation for Optic Nerve Disease, the UK NIH Research (NIHR) as part of the Rare Diseases Translational Research Collaboration, the NIHR Cambridge Biomedical Research Centre (BRC-1215-20,014), and the NIHR Biomedical Research Centre based at Moorfields Eye Hospital National Health Service (NHS) Foundation Trust and University College London (UCL) Institute of Ophthalmology. The views expressed are those of the author(s) and not necessarily those of the NHS, the NIHR, or the

Department of Health. The study was supported by NIH grant RO1-HL142271 to G.H. and FONDECYT grants 1150677 and 1191770 to V.E.

Author affiliations: [a]Departamento Biología Celular y Molecular, Facultad de Ciencias Biológicas, Pontificia Universidad Católica de Chile, Santiago 8331150, Chile; [b]MitoCare Center for Mitochondrial Imaging Research and Diagnostics, Department of Pathology and Genomic Medicine, Thomas Jefferson University, Philadelphia, PA 19107; [c]Departamento Biomédico, Facultad de Ciencias de la Salud, Universidad de Antofagasta, Antofagasta 1240000, Chile; [d]Wellcome Trust for Mitochondrial Research, Institute of Genetic Medicine, Newcastle University, Newcastle NE2 4HH, UK; [e]John Van Geest Cambridge Centre for Brain Repair, Department of Clinical Neurosciences, University of Cambridge, Cambridge CB2 0PY, UK; [f]Mitochondrial Research Council Mitochondrial Biology Unit, Department of Clinical Neurosciences, University of Cambridge, Cambridge CB2 0XY, UK; [g]Cambridge Eye Unit, Addenbrooke's Hospital, Cambridge University Hospitals, Cambridge CB2 0QQ, UK; [h]University College London Institute of Ophthalmology, University College London, London EC1V 9EL, UK; and [i]Moorfields Eye Hospital National Health Service Foundation Trust, London EC1V 2PD, UK

Author conxtributions: B.C.-S., D.L., J.M., R.H., P.Y.-W.-M., G.H., and V.E. designed research; B.C.-S., D.L., J.M., and V.E. performed research; B.C.-S., D.L., J.M., D.A., F.B., M.K.S.-H., M.E.A., R.H., P.Y.-W.-M., and V.E. contributed new reagents/analytic tools; B.C.-S., D.L., J.M., F.B., P.Y.-W.-M., G.H., and V.E. analyzed data; and B.C.-S., R.H., P.Y.-W.-M., G.H., and V.E. wrote the paper.

1. A. Olichon *et al.*, Loss of OPA1 perturbates the mitochondrial inner membrane structure and integrity, leading to cytochrome c release and apoptosis. *J. Biol. Chem.* **278**, 7743–7746 (2003).
2. G. Twig *et al.*, Fission and selective fusion govern mitochondrial segregation and elimination by autophagy. *EMBO J.* **27**, 433–446 (2008).
3. E. S. Ramos *et al.*, Mitochondrial fusion is required for regulation of mitochondrial DNA replication. *PLoS Genet.* **15**, 1–28 (2019).
4. M. Giacomello, A. Pyakurel, C. Glytsou, L. Scorrano, The cell biology of mitochondrial membrane dynamics. *Nat. Rev. Mol. Cell Biol.* **21**, 204–224, (2020), 10.1038/s41580-020-0210-7.
5. V. Eisner, M. Picard, G. Hajnóczky, Mitochondrial dynamics in adaptive and maladaptive cellular stress responses. *Nat. Cell Biol.* **20**, 755–765 (2018), http://www.ncbi.nlm.nih.gov/pubmed/29950571.
6. Z. Song, M. Ghochani, J. M. McCaffery, T. G. Frey, D. C. Chan, Mitofusins and OPA1 mediate sequential steps in mitochondrial membrane fusion. *Mol. Biol. Cell* **20**, 3525–3532 (2009), http://www.molbiolcell.org/cgi/doi/10.1091/mbc.E09-03-0252.
7. X. Liu, D. Weaver, O. Shirihai, G. Hajnóczky, Mitochondrial "kiss-and-run": Interplay between mitochondrial motility and fusion-fission dynamics. *EMBO J.* **28**, 3074–3089 (2009), http://www.ncbi.nlm.nih.gov/pubmed/19745815.
8. H. Chen *et al.*, Mitochondrial fusion is required for mtDNA stability in skeletal muscle and tolerance of mtDNA mutations. *Cell* **141**, 280–289 (2010).
9. D. Weaver *et al.*, Distribution and apoptotic function of outer membrane proteins depend on mitochondrial fusion. *Mol. Cell* **54**, 870–878 (2014).
10. M. E. Harner *et al.*, An evidence based hypothesis on the existence of two pathways of mitochondrial crista formation. *Elife* **5**, e18853 (2016).
11. C. Delettre *et al.*, Nuclear gene OPA1, encoding a mitochondrial dynamin-related protein, is mutated in dominant optic atrophy. *Nat. Genet.* **26**, 207–210 (2000).
12. G. J. K. Praefcke, H. T. McMahon, The dynamin superfamily: Universal membrane tubulation and fission molecules? *Nat. Rev. Mol. Cell Biol.* **5**, 133–147 (2004).
13. C. Delettre *et al.*, Mutation spectrum and splicing variants in the OPA1 gene. *Hum. Genet.* **109**, 584–591 (2001).
14. A. Olichon *et al.*, OPA1 alternate splicing uncouples an evolutionary conserved function in mitochondrial fusion from a vertebrate restricted function in apoptosis. *Cell Death Differ.* **14**, 682–692 (2007).
15. Z. Song, H. Chen, M. Fiket, C. Alexander, D. C. Chan, OPA1 processing controls mitochondrial fusion and is regulated by mRNA splicing, membrane potential, and Yme1L. *J. Cell Biol.* **178**, 749–755 (2007).
16. L. Pernas, L. Scorrano, Mito-morphosis: Mitochondrial fusion, fission, and cristae remodeling as key mediators of cellular function. *Annu. Rev. Physiol.* **78**, annurev-physiol-021115-105011 (2015), https://doi.org/10.1146/annurev-physiol-021115-105011.
17. T. MacVicar, T. Langer, OPA1 processing in cell death and disease – the long and short of it. *J. Cell Sci.* **129**, 2297–2306 (2016), 10.1242/jcs.159186.
18. R. M. DeVay *et al.*, Coassembly of Mgm1 isoforms requires cardiolipin and mediates mitochondrial inner membrane fusion. *J. Cell Biol.* **186**, 793–803 (2009).
19. T. Ban *et al.*, Molecular basis of selective mitochondrial fusion by heterotypic action between OPA1 and cardiolipin. *Nat. Cell Biol.* **19**, 856–863 (2017).
20. C. Frezza *et al.*, OPA1 controls apoptotic cristae remodeling independently from mitochondrial fusion. *Cell* **126**, 177–189 (2006).
21. M. Barrera, S. Koob, D. Dikov, F. Vogel, A. S. Reichert, OPA1 functionally interacts with MIC60 but is dispensable for crista junction formation. *FEBS Lett.* **590**, 3309–3322 (2016).
22. E. D. Wong *et al.*, The intramitochondrial dynamin-related GTPase, Mgm1p, is a component of a protein complex that mediates mitochondrial fusion. *J. Cell Biol.* **160**, 303–311 (2003).
23. T. Landes *et al.*, OPA1 (dys)functions. *Semin. Cell Dev. Biol.* **21**, 593–598 (2010).
24. V. Del Dotto, M. Fogazza, V. Carelli, M. Rugolo, C. Zanna, Eight human OPA1 isoforms, long and short: What are they for? *Biochim. Biophys. Acta (BBA) Bioenerget.* **1859**, 263–269 (2018).
25. V. Del Dotto *et al.*, OPA1 isoforms in the hierarchical organization of mitochondrial functions. *Cell Rep.* **19**, 2557–2571 (2017).
26. B. Cartes-Saavedra, OPA1 modulates mitochondrial Ca2+ uptake through ER-mitochondria coupling. *Front. Cell Dev. Biol [Internet].* (2022) Jan 3; 9(January): 1–17. Available from: https://www.frontiersin.org/articles/10.3389/fcell.2021.774108/full.
27. V. J. Davies *et al.*, Opa1 deficiency in a mouse model of autosomal dominant optic atrophy impairs mitochondrial morphology, optic nerve structure and visual function. *Hum. Mol. Genet.* **16**, 1307–1318 (2007).
28. M. Votruba *et al.*, Clinical features in affected individuals from 21 pedigrees with dominant optic atrophy. *Arch. Ophthalmol.* **116**, 351–358 (1998).
29. P. Yu-Wai-Man *et al.*, The prevalence and natural history of dominant optic atrophy due to OPA1 mutations. *Ophthalmology* **117**, 1538–1546.e1, (2010), 10.1016/j.ophtha.2009.12.038.
30. P. Yu-Wai-Man *et al.*, Multi-system neurological disease is common in patients with OPA1 mutations. *Brain* **133**, 771–786 (2010).
31. P. Yu-Wai-Man, M. I. Trenell, K. G. Hollingsworth, P. G. Griffiths, P. F. Chinnery, OPA1 mutations impair mitochondrial function in both pure and complicated dominant optic atrophy. *Brain* **134**, 1–5 (2011).
32. B. Le Roux *et al.*, OPA1: 516 unique variants and 831 patients registered in an updated centralized Variome database. *Orphanet. J. Rare Dis.* **14**, 214 (2019).
33. M. J. Landrum *et al.*, ClinVar: Improving access to variant interpretations and supporting evidence. *Nucleic Acids Res.* **46**, D1062–D1067 (2018).
34. S. L. Wolin, L. E. Maquat, Cellular RNA surveillance in health and disease. *Science* **366**, 822–827 (2019).
35. A. Ścieżyńska, Processing of OPA1 with a novel N-terminal mutation in patients with autosomal dominant optic atrophy: Escape from nonsense-mediated decay. Janecke AR, editor. *PLoS One*. **12**, e0183866 (2017).
36. F. Burté, V. Carelli, P. F. Chinnery, P. Yu-Wai-Man, Disturbed mitochondrial dynamics and neurodegenerative disorders. *Nat. Rev. Neurol.* **11**, 11–24 (2014).
37. M. Darshi *et al.*, ChChd3, an inner mitochondrial membrane protein, is essential for maintaining Crista integrity and mitochondrial function. *J. Biol. Chem.* **286**, 2918–2932 (2011).
38. A. Olichon *et al.*, Mitochondrial dynamics and disease, OPA1. *Biochim. Biophys. Acta Mol. Cell Res.* **1763**, 500–509 (2006).
39. V. R. Akepati *et al.*, Characterization of OPA1 isoforms isolated from mouse tissues. *J. Neurochem.* **106**, 372–383 (2008).
40. A. Olichon *et al.*, Effects of OPA1 mutations on mitochondrial morphology and apoptosis: Relevance to ADOA pathogenesis. *J. Cell Physiol.* **211**, 423–430 (2007).
41. P. Amati-Bonneau *et al.*, OPA1 R445H mutation in optic atrophy associated with sensorineural deafness. *Ann. Neurol.* **58**, 958–963 (2005).
42. D. A. Patten *et al.*, OPA1-dependent cristae modulation is essential for cellular adaptation to metabolic demand. *EMBO J.* **33**, 2676–2691 (2014).
43. L. Zimmermann *et al.*, A completely reimplemented MPI bioinformatics toolkit with a new HHpred server at its core. *J. Mol. Biol.* **430**, 2237–2243 (2018).
44. M. D. Hartmann, Functional and structural roles of coiled coils. *Subcell. Biochem.*, **82**, 63–93 (2017).
45. C. Glytsou *et al.*, Optic atrophy 1 is epistatic to the core MICOS component MIC60 in Mitochondrial Cristae shape control. *Cell Rep.* **17**, 3024–3034 (2016), http://linkinghub.elsevier.com/retrieve/pii/S2211124716316229.
46. T. Ban, J. A. W. Heymann, Z. Song, J. E. Hinshaw, D. C. Chan, OPA1 disease alleles causing dominant optic atrophy have defects in cardiolipin-stimulated GTP hydrolysis and membrane tubulation. *Hum. Mol. Genet.* **19**, 2113–2122 (2010).
47. S. A. Samant *et al.*, SIRT3 deacetylates and activates OPA1 to regulate mitochondrial dynamics during stress. *Mol. Cell Biol.* **34**, 807–819 (2014).
48. R. Anand *et al.*, The i-AAA protease YME1L and OMA1 cleave OPA1 to balance mitochondrial fusion and fission. *J. Cell Biol.* **204**, 919–929 (2014).
49. J. Lavie *et al.*, Ubiquitin-dependent degradation of mitochondrial proteins regulates energy metabolism. *Cell Rep.* **23**, 2852–2863 (2018).
50. B. Cho *et al.*, Constriction of the mitochondrial inner compartment is a priming event for mitochondrial division. *Nat. Commun.* **8**, 15754 (2017).
51. C. Yu *et al.*, Structural insights into G domain dimerization and pathogenic mutation of OPA1. *J. Cell Biol.* **219**, e201907098 (2020), https://doi.org/10.1083/jcb.201907098.
52. L. Griparic, N. N. Van Der Wel, I. J. Orozco, P. J. Peters, A. M. van der Bliek, Loss of the intermembrane space protein Mgm1/OPA1 induces swelling and localized constrictions along the lengths of mitochondria. *J. Biol. Chem.* **279**, 18792–18798 (2004).
53. H. Lee, Y. Yoon, Transient contraction of mitochondria induces depolarization through the inner membrane dynamin OPA1 protein. *J. Biol. Chem.* **289**, 11862–11872 (2014).
54. E. Cretin *et al.*, High-throughput screening identifies suppressors of mitochondrial fragmentation in OPA1 fibroblasts. *EMBO Mol. Med.* **13**, e13579 (2021).
55. R. G. Abrisch, S. C. Gumbin, B. T. Wisniewski, L. L. Lackner, G. K. Voeltz, Fission and fusion machineries converge at ER contact sites to regulate mitochondrial morphology. *J. Cell Biol.* **219** (2020).
56. N. H. Fukushima, E. Brisch, B. R. Keegan, W. Bleazard, J. M. Shaw, The GTPase effector domain sequence of the Dnm1p GTPase regulates self-assembly and controls a rate-limiting step in mitochondrial fission. *Mol. Biol. Cell.* **12**, 2756–2766 (2001).
57. R. Ramachandran, S. L. Schmid, The dynamin superfamily. *Curr. Biol.* **28**, R411–R416 (2018).
58. D. Li, J. Wang, Z. Jin, Z. Zhang, Structural and evolutionary characteristics of dynamin-related GTPase OPA1. *PeerJ* **2019**, 1–18 (2019).
59. K. Faelber *et al.*, Structure and assembly of the mitochondrial membrane remodelling GTPase Mgm1. *Nature* **571**, 429–433 (2019).
60. V. del Dotto *et al.*, Deciphering OPA1 mutations pathogenicity by combined analysis of human, mouse and yeast cell models. *Biochim. Biophys. Acta Mol. Basis Dis.* **1864**, 3496–3514 (2018).
61. C. Zanna *et al.*, OPA1 mutations associated with dominant optic atrophy impair oxidative phosphorylation and mitochondrial fusion. *Brain* **131**, 352–367 (2008).
62. V. Eisner, G. Lenaers, G. Hajnóczky, Mitochondrial fusion is frequent in skeletal muscle and supports excitation-contraction coupling. *J. Cell Biol.* **205**, 179–195 (2014).
63. B. A. Wilson, A. Ramanathan, C. F. Lopez, Cardiolipin-dependent properties of model mitochondrial membranes from molecular simulations. *Biophys. J.* **117**, 429–444 (2019).
64. C. Bocca *et al.*, Lipidomics reveals triacylglycerol accumulation due to impaired fatty acid flux in Opa1 -disrupted fibroblasts. *J. Proteome. Res.* **18**, 2779–2790 (2019).
65. K. Mohanraj *et al.*, Inhibition of proteasome rescues a pathogenic variant of respiratory chain assembly factor COA7. *EMBO Mol. Med.* **11**, 1–21 (2019).
66. P. M. Quirós, T. Langer, C. López-Otín, New roles for mitochondrial proteases in health, ageing and disease. *Nat. Rev. Mol. Cell Biol.* **16**, 345–359 (2015).
67. C. S. Benjamín *et al.*, Western blot uncropped files. Open Science Framework. https://osf.io/ejp7t/?view_only=e23eb621818540a99d7b5ed304a4e7f7. Deposited 6 May 2022.